www.czasopisma.pan.pl PAN POLSKA AKADEMIA NAUK www.journals.pan.pl

ARCHIVE OF MECHANICAL ENGINEERING

DOI: 10.24425/ame.2025.154739 2025, Vol. 72, No. 2, pp. 359–377

Mirosław RODZEWICZ [1], Bartlomiej Jacek KUBICA [2]

Determining a representative load spectrum for a photogrammetric mission of a lightweight unmanned aircraft

Received 28 February 2025, **Revised** 22 June 2025, **Accepted** 30 June 2025, **Published online** 4 July 2025

Keywords: load spectra, unmanned aircraft, photogrammetry mission, fatigue life

The article investigates the load spectrum of an unmanned aircraft, leveraging autopilot logs from UAV photogrammetry flights over King George Island in Antarctica. The recorded acceleration signals from these logs were converted into a load factor time series, which served as the basis for processing the load spectra. Each flight's load signal was transformed into a sequence of local extremes of Load Levels by dividing the range of operational load variability into 32 intervals. Utilizing the Rainflow Counting Algorithm, a set of half-cycle arrays and the resulting incremental load spectra were obtained. By analyzing the frequency of individual load increments over one hour of flight, three representative load spectra for the entire flight session were developed, each with varying degrees of conservatism. The most conservative spectrum was created by enveloping a set of load half-cycle arrays from all flights. To apply this load spectrum for fatigue tests, a computer program was developed to reconstruct the load sequence from the input transfer array. Finally, fatigue life was calculated, and the effects of applying each developed load spectrum were compared. The article underscores the significance of the obtained load spectra for both fatigue calculations and programming fatigue tests.

Nomenclature

NOTE: In all the designations mentioned below, the index "1h" indicates that the given value is related to 1 hour of flight.

aggregated LS (or LS_agg)	an average load spectrum of the whole flight session
FC-array or **FCA**	a full cycle array
HC-array or **HCA**	a half cycle array

✉ Mirosław RODZEWICZ, e-mail: miroslaw.rodzewicz@pw.edu.pl

[1] Warsaw University of Technology, Warsaw, Poland

[2] Warsaw University of Life Sciences, Warsaw, Poland

HCA_1*h*_agg	an array of the aggregated load spectrum from the whole flight session
HCA_1h_env	an envelope of the **HCA**_1*h* arrays from each flight of the flight session
HCA_1*h*_wenv	a weighted envelope of the **HCA**_1*h* arrays from each flight of the flight session
ILS	an incremental load spectrum; (ILSs = plural form)
LL_LE	local extremes of the load signal
LS	a load spectrum; (LSs = plural form)
LS envelope (or LS_env)	an envelope of the load spectrum from the whole flight session
n_1*h*_Δ	hourly number of load half-cycles calculated separately for the currently considered ΔLL value
n_1*h*_C	hourly number of load half-cycles counted cumulatively, starting from the highest ΔLL value down to the currently considered ΔLL value
N-array	an array of the number of cycles to failure
n_z	load factor
n_{z_max} and n_{z_min}	extreme operating load limits
Δn_z	a load factor increment
LL	a load level (load represented as an integer number in 32-step scale covering the operational load range)
ΔLL	a load level increment, when a load signal transfers to a next local extremum
PSE	a principal structural element
t_f	time of an f-indexed flight
t_T	total time of the whole flight session
$w_{\Delta LL}$	weighting coefficient

1. Introduction

The interest of scientists and engineers in the durability and fatigue of unmanned aerial vehicle (UAV) structures is gradually increasing alongside the growing popularity of this type of aviation [1–3]. The foundation of all fatigue testing is the information on the load spectra acting on the aircraft's load-bearing structure. In manned aviation, these matters have been well-researched, beginning with studies conducted in Germany before World War II [4], and extending through extensive research on General Aviation aircrafts conducted from the 1960s to the 1990s by NASA [5, 6]. As a result of these studies, standard load spectra for fatigue life calculations and fatigue testing of aircraft structures have been developed. Additionally, numerical tools for programming fatigue tests have been created, featuring the intriguing aspect of including probabilistic distributions alongside specific deterministic parameters. These distributions pertain to factors such as the number of exceedances of various load levels due to maneuvers or gusts, making the generated load programs resemble "natural" aircraft loads as well as the S-N curves [7]. An example of a professional suite of such tools is SMART, developed at the University

of Texas at San Antonio [8]. Research in this field is ongoing, as demonstrated by selected works on aircraft load spectra. These efforts focus on reducing the time and costs associated with full-scale fatigue testing through the use of "accelerated load spectra" [9] and the publication [10] on simplification methods for multi-level load spectra.

Studies on methods for determining the fatigue life of unmanned aircraft and the standardization of these methods are in the development phase.

An example of a publication providing a comprehensive analysis of the fatigue life of structures in large and medium-sized UAVs, based on load spectrum and probabilistic cracking mechanisms, is referenced in work [11].

This article focuses on the method of determining the representative load spectrum for a photogrammetric mission of a lightweight unmanned aircraft. The subject of the authors' interest is the unmanned aerial vehicle PW-ZOOM (Fig. 1), constructed at the Warsaw University of Technology [12]. Technical data of this plane are displayed in Tab. 1. The PW-ZOOM was developed as a part of the MONICA project implementation. This project was carried out between 2014 and 2016 under a Polish-Norwegian grant, dedicated to monitoring of Antarctic ecosystems [13]. During three Antarctic expeditions, the PW-ZOOM aircraft covered a distance of 3,641 kilometers, spending over 29 hours in the air and capturing approximately 24,000 orthophotographs of Antarctic Specially Protected Areas (ASPA 128 and ASPA 151) located on King George Island (the largest of the South Shetland Islands), which were used to create orthophotomaps or numerical models of the terrain. Despite the passage of time, this achievement remains notable for its extensive use of unmanned aircraft in monitoring of Antarctic ecosystems.

One of the valuable remnants of the MONICA project is the collection of autopilot logs from completed photogrammetric missions. The data for the analysis

Fig. 1. The PW-ZOOM – preparation for take-off from Antarctic Station Arctowski

Table 1. Main technical data of the PW-ZOOM

Wing span	3.19 m
Wing area	1.28 m^2
Wing airfoil	Eppler E-205
Optimal cruise speed	100–110 km/h
Max. speed of horizontal flight	160 km/h
Max. take-off weight	23 kg
Payload	3.5 kg
Max. tolerable wind speed	23 m/s
Autopilot	MP2128g
Telemetry communication range	30 km
Engine	2-stroke 3.58 kW
Propeller	$19x10''$
Fuel	2.2l tank or 4.5l extended tank with 95 octane gasoline/2-stroke oil 30:1 mixture
Max. operational range	160 km (330 km with extended tank mounted instead of parachute system)

presented in this paper comprised load spectra from 23 photogrammetric flights conducted by the PW-ZOOM during Antarctic expeditions in 2014, 2015 and 2016 (Fig. 2 and Fig. 3). The PW-ZOOM aircraft were equipped with Micropilot

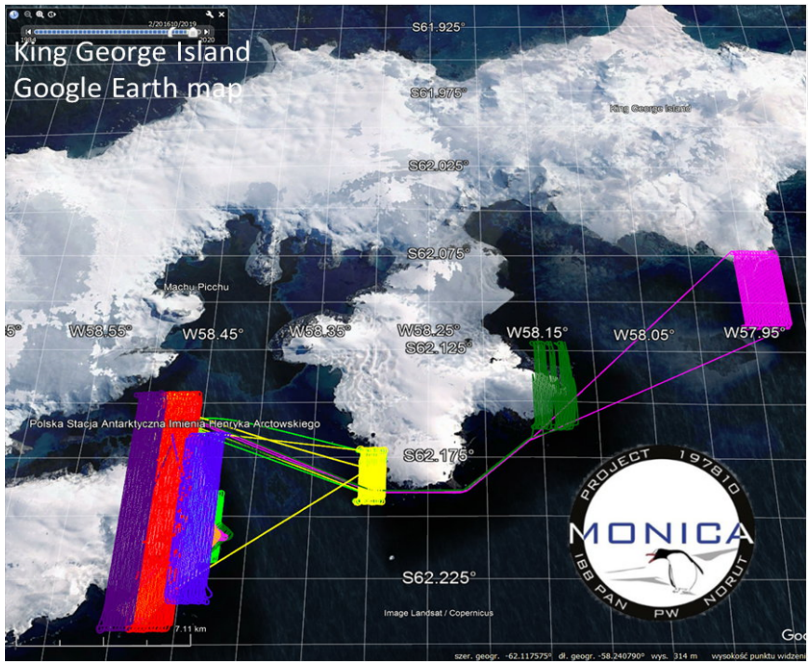

Fig. 2. GPS flight paths of 23 flights of PW-ZOOM over the KGI

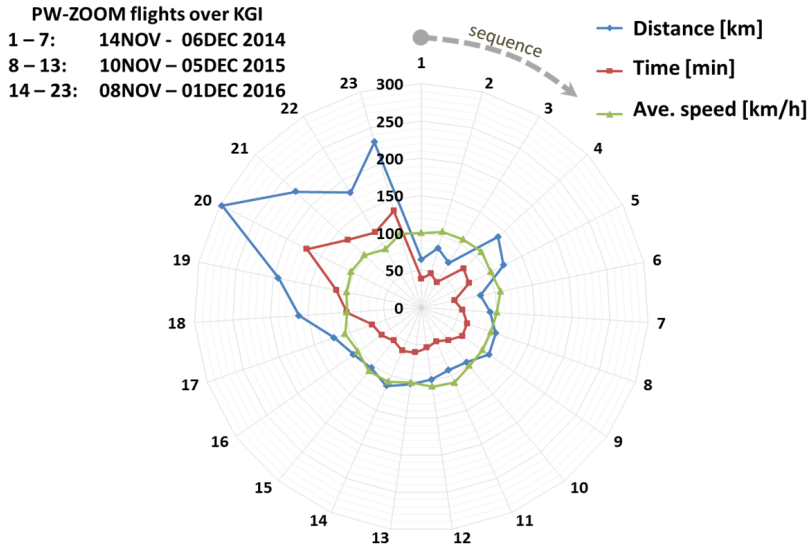

Fig. 3. PW-ZOOM flight data chart

MP2128g autopilots that generate logs recorded at a frequency of 5Hz. These autopilot logs contain a wealth of information regarding the dynamic behaviors of the aircraft, such as spatial orientation angles, linear and angular velocities, accelerations, and more. Additionally, they include flight paths recorded by GPS systems, control signal logs, and other data. This study utilizes the acceleration signal records along the z-axis (az acceleration). The time series of this acceleration allow for the development of load spectra acting on the primary load-bearing structure of the aircraft (i.e., wings and their attachment system to the fuselage).

2. Acceleration signal srocessing

Acceleration signal processing involves several steps (Fig. 4). The first step is converting a sequence of real numbers, which represents the az acceleration values recorded at a sampling frequency of 5Hz, into a sequence of integers ranging from 1 to 32. These integers represent the so-called Load Levels (LL). The conversion from acceleration to LL adheres to the standard formula established by the pioneers of using tabular forms for presenting load spectra [4]:

$$\text{for} \quad n_{z\_max}\text{LL} = 3 \quad \text{and for} \quad n_{z\_min}\text{LL} = 31, \tag{1}$$

where $n_z = a_z/g$. The range of permissible operational loads for the aircraft is between $3 \leqslant \text{LL} \leqslant 31$. The load levels LL = 1, 2 and 32 are reserved for recording incidental-minor exceedances beyond the allowed operational range (which are undesirable but may occur unintentionally against the aircraft operators' will).

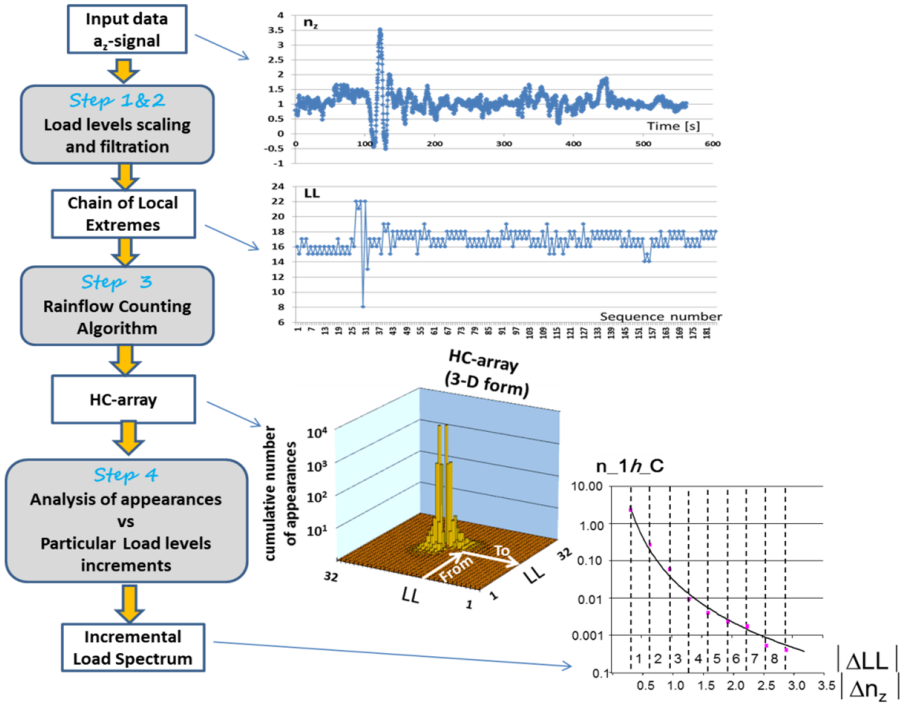

Fig. 4. Diagram of the load spectrum derivation algorithm

The second step involves filtering the sequence of LL values into a sequence of LL local extremes (LL_LE). In this sequence, for any three consecutive elements, if the transition from one value to the next involves an increase in LL, then the transition between the second and third value must involve a decrease in LL, and vice versa.

The third step is to apply the Rainflow Counting algorithm to analyze the LL_LE sequence and generate a so-called half-cycle array (**HC-array**) with dimensions of 32×32. This array is a specific form of the transfer array, where the subsequent transitions of the LL_LE signal are recorded according to the principle "from the LL to the LL" (where "from the LL" refers to the row number and "to the LL" refers to the column number shown in Fig. 4). In both arrays, the diagonals connecting the cells with indices 1,1 and 32,32 are called the "zero-diagonal". The **HC-array** differs from the regular transfer array by incorporating the Rainflow Counting algorithm, which counts the resultant increases in the load signal caused by the sequence of successive changes in the LL_LE signal [15, 16]. A common feature of both arrays (besides having the same graphical layout) is that the sum of all load signal transfers recorded in the cells of the transfer array and of the **HC-array** is equal and corresponds to the total number of local extremes in the LL_LE sequence minus 1. Also, the "active zone" of both arrays (defined as the envelope of columns and rows containing at least one non-zero value, typically

forming a rectangular shape) is identical. This property is used as one of the checks for the correctness of the calculations performed. For the simplification of fatigue calculations, the **HC-array** can be transformed into a full-cycle array (**FC-array**), which contains the number of load cycles on only one side of the "zero diagonal". It is important to note that one full cycle consists of two half-cycles: one associated with a load increase and the other with a load decrease. They are represented in the **HC-array** as a pair of cells positioned on the opposite side of the "zero-diagonal" (for example indexed as j, i and i, j).

The fourth step is to create incremental load spectra, which are very helpful for comparing load spectra from different flights.

To successfully implement the 4-step signal processing procedure discussed above, it needs to be integrated into a computer program. An example of such an implementation is the SPECTRA program, developed in the LabVIEW environment [17].

3. Analysis of load spectra from PW-ZOOM aircraft photogrammetric flights

The PW-ZOOM flights were conducted under varying atmospheric conditions. The weather in the King George Island area is known for its rapid changes, necessitating the identification of "weather windows" suitable for flying. Additionally, the flights had to be scheduled around the breeding calendar of various penguin species. Consequently, flights sometimes had to be carried out in less favorable conditions, such as strong winds or lower cloud ceilings, which could cause increased turbulence and affect the aircraft's flight dynamics.

Due to the fact that the acceleration signal can be correlated with the aircraft wing loads only in flight phases without contact with the ground [18], the analysis presented in this article took into account only the time intervals from the moment the airplane left the take-off catapult to the moment just before landing. Using the algorithm presented in Fig. 4, calculations were performed for each flight, resulting in 23 **HC-arrays** and corresponding **FC-arrays**. Using the normalization formula (1), the following load factor limit values were applied: $n_{z\_max} = 5$; $n_{z\_min} = -3$.

The **FC-arrays** were necessary to generate single-branch incremental load spectra, which served as the basis for further analysis. Sample results for determining **FC-arrays** are shown in Fig. 5. They pertain to two flights conducted along the same route under different atmospheric conditions. An increase in the so-called "active zone" of the **HC-array** (marked here in yellow) due to turbulence caused by strong winds is evident. Since it is challenging to clearly present the values of the cells in a full-size 32×32 table, ASCII codes for LL load levels were used to represent the "active zones" on the "zero-diagonals", with A corresponding to 1, B to 2, and so on.

A set of 23 **HC-arrays** and corresponding **FC-arrays** were used to develop a load spectrum representative of an entire flight session encompassing all 23

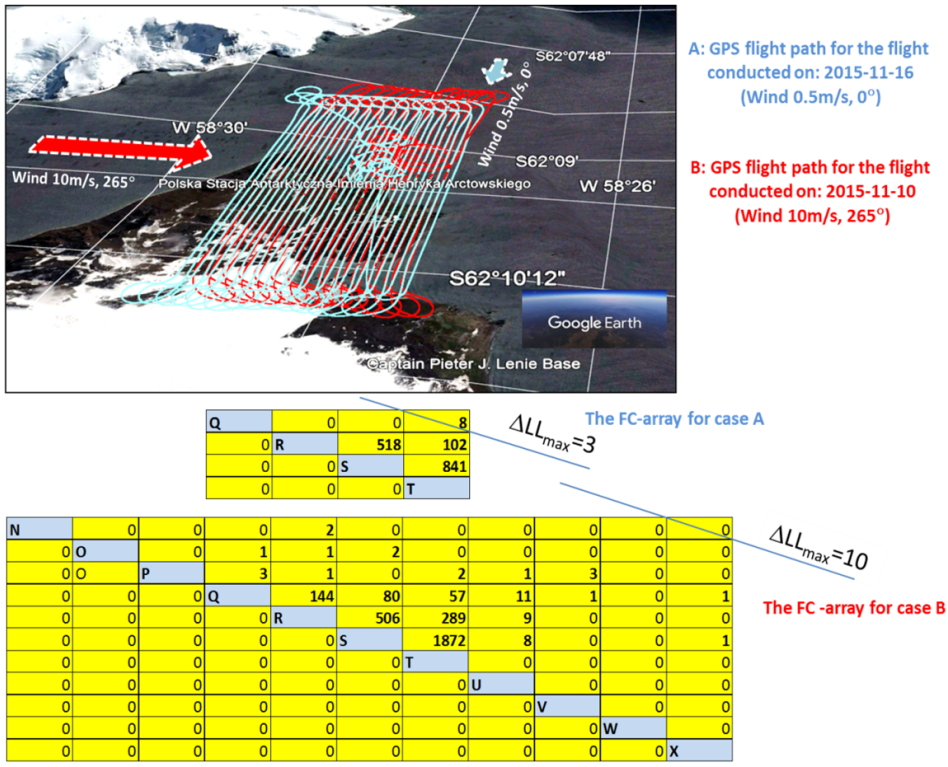

Q			0	0	8					
	0	R		518	102					
	0		0	S	841					
	0		0		0	T				

N	0	0	0	2	0	0	0	0	0	0
0	O	0	1	1	2	0	0	0	0	0
0	O	P	3	1	0	2	1	3	0	0
0	0	0	Q	144	80	57	11	1	0	1
0	0	0	0	R	506	289	9	0	0	0
0	0	0	0	0	S	1872	8	0	0	1
0	0	0	0	0	0	T	0	0	0	0
0	0	0	0	0	0	0	U	0	0	0
0	0	0	0	0	0	0	0	V	0	0
0	0	0	0	0	0	0	0	0	W	0
0	0	0	0	0	0	0	0	0	0	X

Fig. 5. Zoom into "active zones" of the **FC-arrays** derived for two similar photogrammetry tasks performed in different wind conditions

flights. This spectrum was created in three different forms. The primary form is the aggregated load spectrum, which averages the load histories from the 23 flights and relates the number of load change occurrences to one hour of the flight session. It is represented by the **HCA**_1h_agg array, where the cell with indices i, j contains the sum of the load half-cycles from the cells with the same indices in the set of 23 **HC-arrays**, divided by the total flight time t_T (see formula (2)).

$$\mathbf{HCA}\_1h\_\mathrm{agg}_{i,j} = \sum_{f=1}^{F} \frac{\mathbf{HCA}\_f_{i,j}}{t_T} = \sum_{f=1}^{F} \left(\mathbf{HCA}\_1h\_f_{i,j} \frac{t_f}{t_T} \right), \tag{2}$$

where i, j are the indices of the cells in a 32×32 array, and f is the flight index relevant to a given HC-array ($f = 1, 2, \ldots, F = 23$).

These indices pertain to formulas (2) through (5). The aggregated LS is presented below in the form of the **FCA**_1h array (Fig. 6).

The second form is the load spectrum envelope. Here, the number of load half-cycles is also referenced to 1 hour of flight. In the **HCA**_env array representing such an LS, the cell at index i, j contains the highest value found in cells with

E	0	0	0	0	0	0	0	0	0	0	0	0	0	0	0.0344	0	0.0344	0
0	F	0	0	0	0	0	0	0	0	0	0	0	0	0	0	0	0	0
0	0	G	0	0	0	0	0	0	0	0	0	0	0	0	0	0	0	0
0	0	0	H	0	0	0	0	0	0	0	0	0	0	0	0	0	0	0
0	0	0	0	I	0	0	0	0	0	0	0	0	0	0	0	0	0	0
0	0	0	0	0	J	0	0	0	0	0	0	0	0	0	0.0344	0.0344	0	0
0	0	0	0	0	0	K	0	0	0	0	0	0	0	0	0	0	0	0
0	0	0	0	0	0	0	L	0	0	0	0	0.0344	0	0.0344	0	0	0	0
0	0	0	0	0	0	0	0	M	0	0	0.0344	0	0.0344	0	0	0	0	0
0	0	0	0	0	0	0	0	0	N	0	0.0344	0.0688	0.1720	0.0688	0.1720	0.0688	0.0344	0
0	0	0	0	0	0	0	0	0	0	O	0.3441	0.3441	0.8258	0.8258	0.7226	0.6882	0.1720	0.0344	0.0344
0	0	0	0	0	0	0	0	0	0	0	P	2.7871	3.7850	3.4753	4.9893	2.3742	1.1011	0.1720	0.0344
0	0	0	0	0	0	0	0	0	0	0	0	Q	74.5986	59.4243	38.9509	9.2560	1.0323	0.1032	0.0344
0	0	0	0	0	0	0	0	0	0	0	0	0	R	589.9072	295.7106	15.6217	0.7226	0.1376	0.0688
0	0	0	0	0	0	0	0	0	0	0	0	0	0	S	1061.0692	11.4238	0.6194	0.034409	0.0688
0	0	0	0	0	0	0	0	0	0	0	0	0	0	0	T	1.3764	0.1376	0.0344	0.0344
0	0	0	0	0	0	0	0	0	0	0	0	0	0	0	0	U	0	0	0
0	0	0	0	0	0	0	0	0	0	0	0	0	0	0	0	0	V	0	0
0	0	0	0	0	0	0	0	0	0	0	0	0	0	0	0	0	0	W	0
0	0	0	0	0	0	0	0	0	0	0	0	0	0	0	0	0	0	0	X

Fig. 6. The „active zone" of the **FCA**_1h_agg representing all 23 flights

the same indices in the set of 23 **HC-arrays**. These arrays contain the number of half-cycles referenced to the flight time corresponding to the given **HC-array**.

$$\mathbf{HCA}\_1h\_\mathrm{env}_{i,j} = \overset{F}{_{f=1}} \max(\mathbf{HCA}\_1h\_f)_{i,j}. \tag{3}$$

The third form is the LS weighted envelope. The **HC-array** representing this spectrum contains the product of the values of the **HCA**_1h_env array cells and the weighting coefficients $w_{\Delta\mathrm{LL}}$. These coefficients have constant values on lines representing specific ΔLL values (i.e., lines parallel to the "zero diagonal" and offset by the ΔLL value). The weighting coefficient value for a given ΔLL depends on the number of flights in which load increments of that value occurred. It is calculated as the ratio of the sum of flight durations, during which a specific ΔLL value occurred, to the total time of all flights t_T. Therefore, if a given ΔLL value occurred in every flight, $w_{\Delta\mathrm{LL}}$ equals 1. If a given ΔLL value occurred in only one flight, $w_{\Delta\mathrm{LL}}$ is the ratio of that flight's time to t_T, which is a small value.

$$\mathbf{HCA}\_1h\_\mathrm{wenv}_{i,j} = \mathbf{HCA}\_1h\_\mathrm{env}_{i,j}\, w_{\Delta\mathrm{LL}}. \tag{4}$$

For $\Delta\mathrm{LL} = k$, where $k = 1, 2, \ldots, 31$ value of $w_{\Delta\mathrm{LL}}$ is given by the following formula:

$$w_{\Delta\mathrm{LL}=k} = \sum_{f=1}^{F} \left(\mathrm{sgn}(n\_1h\_\Delta_f)_{\Delta\mathrm{LL}=k} \frac{t_f}{t_T} \right). \tag{5}$$

A comparison of the incremental LS for the three forms described above is shown in Fig. 7. It can be observed that the highest frequency of various ΔLL occurrences per flight-hour for each ΔLL value occur in the LS-envelope. This

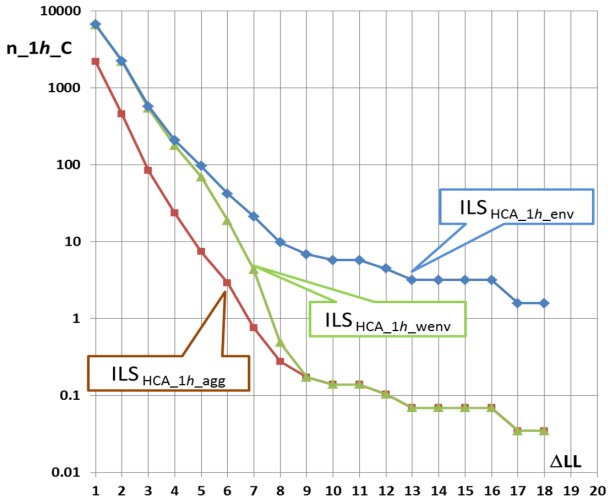

Fig. 7. The ILSs representing the LS_1*h* envelope (blue line), aggregated LS (red line), and LS_1*h* weighted envelope (green line) from all 23 flights

load spectrum is thus the most conservative, as it assumes that for each ΔLL in every flight the highest frequency observed during the analyzed flight session will occur.

In contrast, the lowest values of various ΔLL occurrences per hour of flight for each ΔLL occur in the LS_agg. This load spectrum is non-conservative because it contains frequencies of ΔLL occurrences averaged over the entire flight session; there occurred flights where these numbers were higher. The line representing LS weighted envelope for large ΔLL values coincides with the line representing the LS_agg and converges with the LS envelope line for small ΔLL values. Therefore, this spectrum is more conservative than the LS_agg and less conservative than the LS_env.

4. Assessment of the conservatism of the load spectrum representative for a given flight session, based on fatigue calculations

The distances between the lines in Fig. 7 demonstrate the quantitative differences in the frequencies of various ΔLL values across individual representations of the load spectrum for the entire flight session. However, it is challenging to predict how this will translate into the fatigue life of the structure subjected to these load spectra. This chapter presents fatigue life calculations considering the fatigue characteristics of the material. The calculations were conducted based on the Palmgren-Miner hypothesis, whose application to estimating the fatigue life of aircraft structures is detailed in Report AFS-120-73-2 [19]. This report posits that the fatigue life of an aircraft structure is constrained by the fatigue durability of its

weakest component within the main load bearing structure, named as the "Principal Structural Element" (PSE). In this study, an updated calculation algorithm was used, involving 32×32 array constructed similarly to the **HC-array** containing the fatigue properties of the material. Consequently, the classical P-M hypothesis formula was modified as follows:

$$\boldsymbol{D} = \chi \sum_{i=1}^{32} \sum_{j=1}^{32} D_{i,j} = \chi \sum_{i=1}^{32} \sum_{j=1}^{32} \frac{n_{i,j}}{N_{i,j}}. \tag{6}$$

Symbol χ is the coefficient equal to 1 or 0.5 depending on the kind of transfer arrays used for calculations (i.e., a **FC-array** or a **HC-array**).

In this formula, $N_{i,j}$ represents a cell in the **N-array** containing the number of load cycles (or half-cycles) to failure, while $n_{i,j}$ denotes a value identical to the content of the **HC-array** cell. For the PW-ZOOM aircraft, the critical element identified as the PSE is the wing connector, which is a metal tube made from an alloy with similar fatigue properties to those described in Report AFS-120-73-2. These properties are presented in the form of S-N curves, showing the number of cycles to failure as a function of the amplitude of variable stress cycles and the mean value of these cycles. When transforming the S-N curves into an **N-array**, it was assumed that the stresses in the PSE are proportional to the n_z value. It was estimated that for $n_z = 1$, the stresses are 26 MPa. Based on this, auxiliary 32×32 arrays were created, containing information on the amplitude (Sa) and mean value of stress (Sm) in the PSE. Based on these data and those from Report AFS-120-73-2, where S-N curves for individual average values of variable stress are shown on a logarithmic scale as a series of straight line segments, the number of cycles to failure for each cell in the **N-array** was determined (Fig. 8). In the **N-array**, the yellow region signifies interpolated values, which fall within empirically verified ranges. Conversely, the white region indicates extrapolated values, extending beyond these verified ranges. For accurate fatigue life calculations, it was crucial that all non-zero cells in the **HC-array** correspond to the marked area cells in the **N-array**. The graph in the Fig. 9 illustrates the results of the fatigue life calculations for each load spectrum depicted in Fig. 7.

As one can see, the fatigue durability calculated for LS labeled as **HCA**_agg is 3.5 times greater than the result obtained for **HCA**_wenv and over 30 times greater than **HCA**_env. It should be noted that these proportions apply only to the aircraft's photogrammetric mission. To ensure the production of high-quality orthophotomaps, the aircraft must maintain a smooth flight along the designated photogrammetric route, avoiding any sharp maneuvers. When these conditions are met, the load variations are minimal compared to the operational load range considered during the aircraft's design process. Higher load exceedances occur only incidentally (e.g., due to encountering turbulence). If the flight session had been dedicated to flights involving aerobatic elements or flights in strong turbulence conditions, the obtained proportions would have changed and the differences in

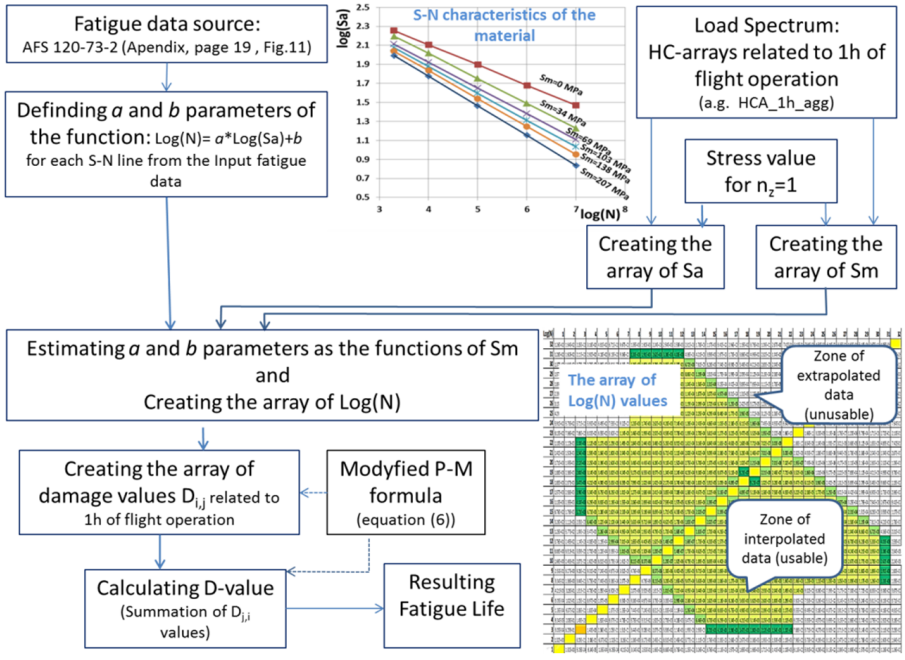

Fig. 8. Schematic diagram of the fatigue life calculation method

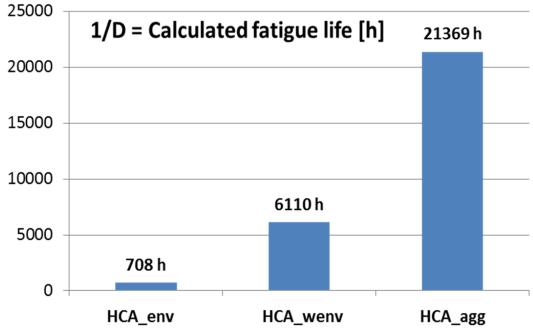

Fig. 9. Results of fatigue life assessment for three load spectra representative of the PW-ZOOM photogrammetric flight session

calculation results for the considered types of load spectra representative of such a flight session would have decreased, with a concurrent reduction in fatigue durability.

5. Load spectrum for experimental validation of fatigue durability

Let's assume hypothetically that we are tasked with confirming the fatigue durability of an aircraft structure used exclusively for photogrammetric missions. To prepare a fatigue test for the aircraft structure, it is necessary to develop a

test program in the form of a sequence of loads to be applied on the test stand. The simplest solution would be to "assemble" sequences of load local extremes (LL_LE) that were generated while creating **HC-arrays** for all flights conducted during the flight session. This approach would mean selecting a **HCA**_agg for the fatigue test implementation.

Experimental verification of fatigue durability must involve conducting fatigue tests using a load spectrum that is conservative enough to ensure that the probability of encountering higher frequency of various ΔLL occurrences per flight-hour during aircraft operation is minimal for all permissible load increments. Therefore, the safest approach would be to use the **HCA**_env load spectrum for testing. Since this array was developed through theoretical considerations and no flight with such a load spectrum has occurred in practice, the main challenge becomes generating a load LL_LE sequence suitable for this spectrum, which can be applied in fatigue testing. This is essentially the reverse operation of creating **HC-arrays**.

Reconstructing the LL_LE sequence involves performing an algorithmic trajectory that passes through all non-zero cells of the HC array [20]. This trajectory features multiple loops that begin and end at the "zero diagonal" in cells designated as "transition gates." These gates are situated at the intersections of rows and columns that contain at least one non-zero value, as illustrated by the pink array cells in Fig. 10. The starting point can be any cell on the “zero diagonal” marked in pink.

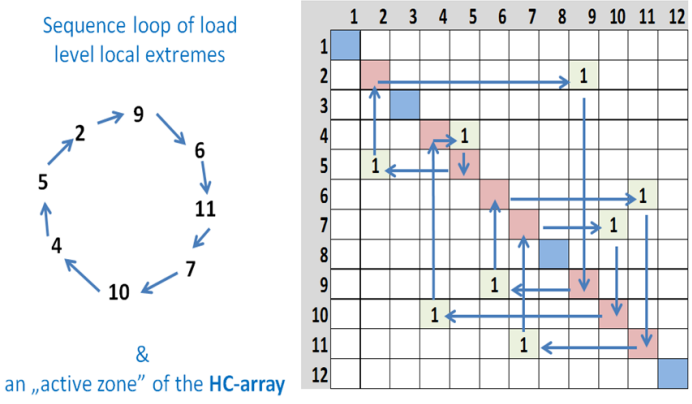

Fig. 10. The trajectory of "exploring" cells on the **HC-array** allowing for the reconstruction of the LL_LE sequence

Such a trajectory can be uniquely realized only in a specific case where each column and each row contains exactly one non-zero cell, and the LL_LE sequence forms a closed loop. In complex cases where multiple transfers are recorded in a single row or column of a table, probabilistic methods, particularly Markov chains, are useful tools. When using transfer arrays to reconstruct load sequences, we deal with a hidden Markov chain, where each state is a pair (s, d); here, s repre-

sents the load level, and d indicates the direction of change, taking binary values. The nature of the process generating the LL_LE sequence is such that individual changes are always alternating: if the load decreased in the previous step, it will increase in the next one. Hidden Markov chains are widely used in fields like text mining, biometrics, and especially automated image recognition [21]. Common algorithms used for their parameterization include the Viterbi and Baum-Welch algorithms [22].

In order to reconstruct the LL_LE sequence, a computer program (called LOT.exe) developed by Dr. B.J.K. (the co-author of the article) was utilized. The algorithm of this program is based on the theory of hidden Markov chains, and it uses a random number generator, so the generated load LL_LE sequences are partially similar but not identical, and each run of the program gives a different result. Fig. 11 shows the operation diagram of the algorithm implemented in the LOT.exe program [20].

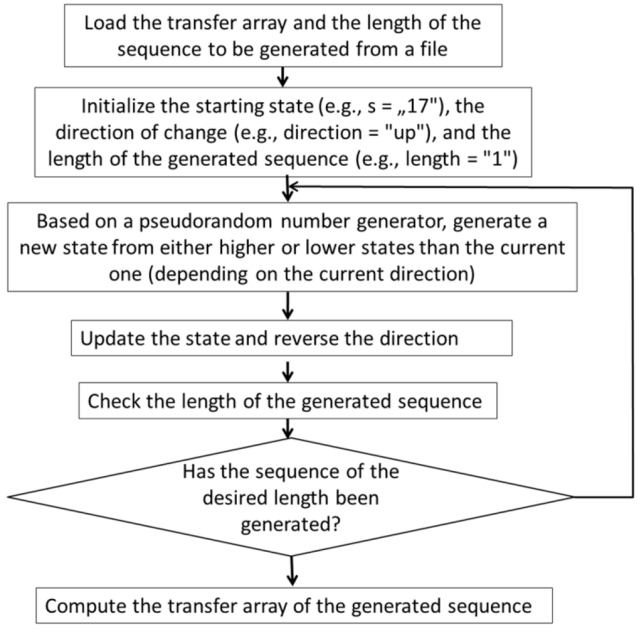

Fig. 11. The algorithm of the load sequence generation program

The sample results are displayed in Fig. 12. On the top is the array labeled **HCA**_29h_in3, which served as input for the LOT.exe program. This array was created by multiplying the **HCA**_1h_env array by the total flight time (t_T = 29.0622 hours) and rounding the results up to the nearest whole numbers. On the bottom is the array **HCA**_29h_in3_out1, which represents the load spectrum obtained from the reconstructed sequence of LL_LE generated by the LOT.exe program.

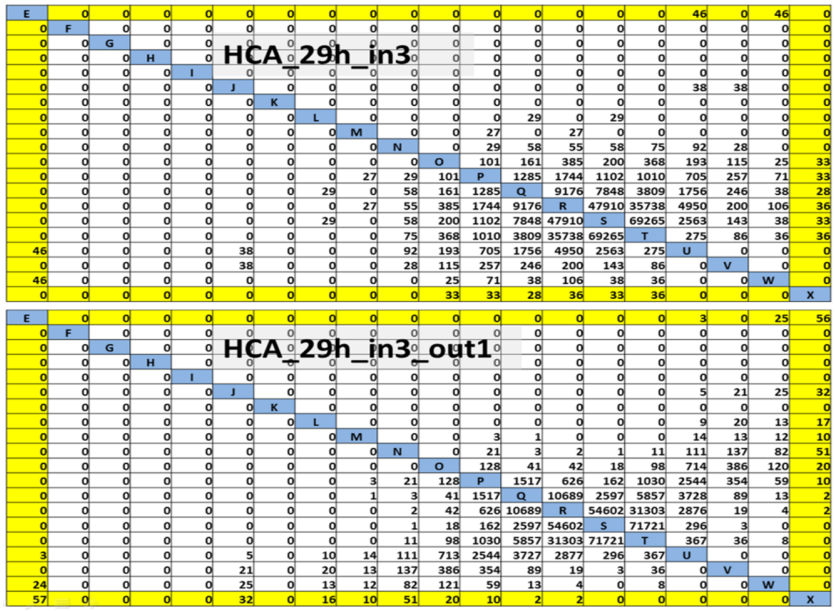

Fig. 12. Comparison of the **HC-arrays**: **HCA**_29h_in3 (i.e., input array) vs **HCA**_29h_in3_out1 (i.e., output array obtained from the reconstructed load sequence)

The sums of the numbers of half-cycles and "active zones" are identical in both arrays, confirming the accuracy of the program's algorithms. Despite differences in cell values at the same indices, there is a notable topological similarity between both arrays. Additionally, the sums of cell values representing individual ΔLL values are comparable in both arrays. This can be verified by comparing the incremental load spectra obtained from both arrays.

The ILS plots derived from both arrays are shown in Fig. 13a. Furthermore, a new plot is included (represented by the green line) that was generated from the load sequence produced during subsequent execution of the LOT.exe program. Relative positions of ILS plots prove that the load spectra derived from the reconstructed load sequences are somewhat more conservative than the input load spectrum. This is evident as the ILS-lines representing reconstructed load sequences lie above the ILS-line representing the input array.

In order to assess the degree of conservatism, fatigue durability calculations were conducted using the same method and computational model as previously described in the text. When comparing obtained results (see fatigue life value in the descriptions of the ILS lines in Fig. 13a) it is evident that the fatigue life values for reconstructed load sequences are lower. Thus, using the load sequence generated by the LOT.exe program as a fatigue test scenario will ensure a comprehensive verification of the aircraft structure concerning fatigue life. It is worth noting that in the generated load sequence none of the loads surpass the permissible operational range. Each generated load sequence contains 385,559 terms, which is one less than

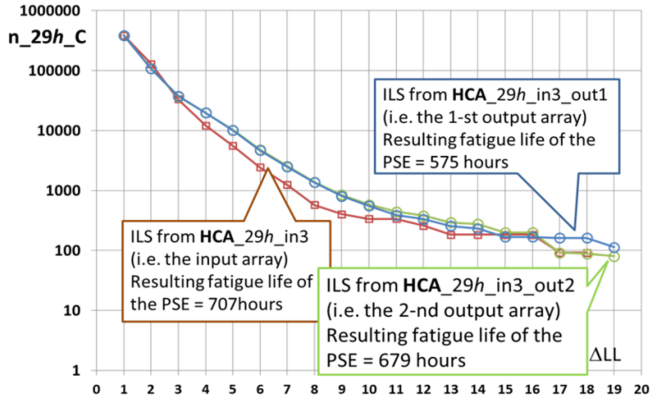

(a)

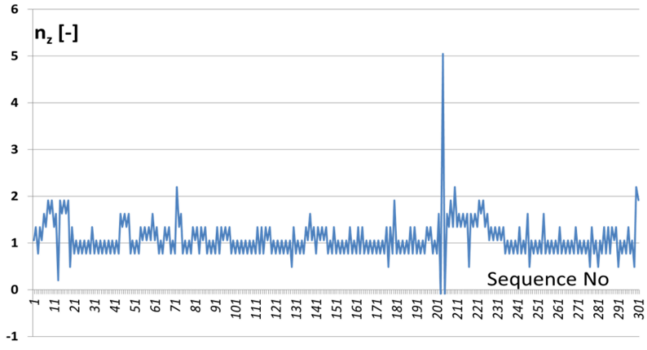

(b)

Fig. 13. Incremental load spectra comparison (a) and the fragment of the generated load sequence (b)

the number of half-cycles in the input array, (i.e., fulfills a necessary condition for a correct solution). The generated load sequence is quasi-stochastic, implying that its application in a fatigue testing system would expose the tested structure to loads comparable to those experienced during actual flights. A fragment of this sequence is shown further in Fig. 13b.

6. Summary and final conclusions

The article outlines methods for determining load spectra representative of unmanned aircraft flight missions. These methods are based on analyzing the extreme frequencies of occurrences of specific ΔLL values within the load half-cycle arrays from all flights in a session. This approach is more conservative than the average load spectrum recorded during the entire measurement session.

It is important to note that the accuracy of estimating the frequency of various load increases, based on a 32-level load scale, relies on the number of flights

analyzed. This study analyzed 23 flights, which are notable due to their operation in Antarctica – however, they do not constitute a sufficiently large data set from a statistical perspective. It is anticipated that if the number of flights increases and includes conditions with more turbulence than those experienced in the analyzed session, the developed load spectra would likely be different.

For the completed flight session, the analytically determined load spectrum, presented as an envelope of the load half-cycle arrays, is highly conservative. This conservatism is manifested in the results of calculations of the fatigue life of a structural element exposed to alternative load spectra, which show that the calculated fatigue life is approximately 30 times lower than the result obtained from the average load spectrum from the flight session.

Less conservative is the load spectrum presented in the form of the weighted envelope of the load half-cycle arrays. If it is applied to the same structural element, then the result of fatigue life calculation is 3.5 times lower than the result obtained from the average load spectrum from the flight session.

The algorithm of a computer program presented in this work, designed to generate quasi-stochastic load sequences from an input transfer array, leads to an increase in the degree of conservatism when its input is provided with an array presenting one of the developed representative load spectra. Two sample load sequences generated by this program resulted in fatigue life calculations that were 1.04 and 1.23 times lower than those derived from the input load half-cycle array. The main reason is that the program's input data, which came from analyzing the extreme frequencies of each individual ΔLL value in the set of load half-cycle arrays from all flights in a session, were influenced by the Rainflow Counting algorithm. As a result, these data included resultant increments in load levels due to the integration of several smaller load level increments.

The variation in the numerical results mentioned in the study arises from the implementation of a random number algorithm in the program, which ensures different outcomes with each execution.

The test results indicate that the methods outlined in this study for creating representative load spectra for a specific flight mission session are user-friendly and provide substantial safety margins. These methods can be easily implemented using Excel, provided there is reliable software available to support the application of the Rainflow Counting algorithm on large datasets, along with a program capable of generating a sequence of local load extremes from the input transfer array.

References

[1] M. Rodzewicz. Airworthiness tests of the UAV structure – fatigue issues. *Fatigue of Aircraft Structures*, 2012(1)82–93, 2012. doi: 10.2478/v10164-012-0060-7.

[2] S.N. Satish Kumar, T.L Rakesh Babu, and M. Ramesh. Fatigue and vibrational analysis of drone by using composite and MMC alloys for military applications. *International Research Journal of Engineering and Technology (IRJET)*, 7(7): 5650–5665, 2020.

[3] Wang Xuanbao, Si Liang, Wang Jiaxing, Wang Zilong, Wang Shuo, Hu Ping, and Duanmu Fanshun, Durability analysis of large and medium-sized unmanned aerial vehicles based on load spectrum and probabilistic fracture mechanics.*Journal of Physics: Conference Series*, 2764 012015, 2023. doi: 10.1088/1742-6596/2764/1/012015.

[4] H.W. Kaul. Die erforderliche Zeit-und Dauerfestigkeit von Flugzeugtragwerken Jarbuch der deutschen Luftfahrtforschlung (The required time and fatigue strength of aircraft structures Jarbuch of German aviation research), pp. 1274–1288, 1938. (in German).

[5] L.E. Clay, R.L. Dickey, M.S. Moran, K.W. Payauys, and T.P. Severyn. Statistical analysis of general aviation VG-VGH data. NASA Report No. NASA-CR-132531. Technology Incorporated Instruments and Control Division, Dayton, Ohio, 1974.

[6] E.J. Locke, H.W. Smith, E.A. Gabriel, and T. DeFlore. General aviation aircraft – normal acceleration data analysis and collection project. Report No DOT/FAA/CT-91/20. University of Kansas Flight Research Laboratory, 1993.

[7] H. Millwater, J. Ocampo, G. Singh, H. Smith, E. Meyer. Probabilistic structural risk assessment and risk management for small airplanes. Report No. DOT/FAA/AR-11/14, Federal Aviation Administration, Kansas City, 2017.

[8] J. Ocampo and H.R. Millwater. SMART|LD (Small Aircraft Risk Technology –Linear Damage Technology and Case Studies Applications. In: *Aircraft Airworthiness & Sustainment Conference*, San Diego, CA, USA, 2011.

[9] X. He, T. Li, Y. Li, Y. Dong, and T. Wang, Developing an accelerated flight load spectrum based on the $n_z - N$ curves of a fleet. *International Journal of Fatigue*, 117:246–256, 2018. doi: 10.1016/j.ijfatigue.2018.08.005.

[10] X. Li and Q. Sun. Simplification approaches for multi-level load spectra by using equivalent damage rule. *Chinese Journal of Aeronautics*, 34(11):119–130, 2021. doi: 10.1016/j.cja.2021.03.025.

[11] X. Wang, L. Si, J. Wang, Z. Wang, S. Wang, P. Hu, and F. Duanmu. Durability analysis of large and medium-sized unmanned aerial vehicles based on load spectrum and probabilistic fracture mechanics. *Journal of Physics: Conference Series*. 2764:012015, 2024. doi: 10.1088/1742-6596/2764/1/012015.

[12] T. Goetzendorf-Grabowski and M. Rodzewicz, Design of UAV for photogrammetric mission in Antarctic area. *Proceedings of the Institution of Mechanical Engineers Part G: Journal of Aerospace Engineering*, 231(9):1660–1675, 2016. doi: 10.1177/0954410016656881.

[13] A. Zmarz, K.S. Rune, M. Kycko, M. Korczak-Abshire, I. Gołębiowska, I. Karsznia, and K. Chwedorzewska. BVLOS UAV missions for vegetation mapping in maritime Antarctic. *Frontiers in Environmental Science*, 11:1–11, 2023. doi: 10.3389/fenvs.2023.1154115.

[14] H. Kossira and W. Reinke. Entwicklung eines Belastungskollektivs fur leichte Motorflugzeuge aus den Beanspruchungsmessungen an einem Segelflugzeug, (Development of a load spectrum for light motor aircraft from the load measurements on a glider), IFL-IB 86-04, TU Braunschweig, 1986.(in German).

[15] M.S. Łukasiewicz. Load spectrum analysis with open source software – an application example. *Fatigue of Aircraft Structures*, 2021(13):17–30, 2022. doi: 10.2478/fas-2021-0003.

[16] S. Gajek. Automation of aircraft fatigue life estimation. *Fatigue of Aircraft Structures*, 2022(14):83–103, 2023. doi: 10.2478/fas-2022-0007.

[17] M. Rodzewicz and D.Głowacki. Investigation into load spectra of UAVs aircraft. *Fatigue of Aircraft Structures*, 2013(5):40–52, 2014. doi: 10.2478/fas-2013-0004.

[18] M. Rodzewicz. Load spectra of a light unmanned aircraft – data recording frequencies and resulting measurement variations, *Archive of Mechanical Engineering*, 71(4):525–545, 2024. doi: 10.24425/ame.2024.151335.

[19] Engineering and Manufacturing Division, Airframe Branch. Fatigue evaluation of wing and associated structure on small airplanes. Report No. AFS-120-73-2, Department of Transportation, Federal Aviation Administration, Washington, DC, USA, 1973.

[20] M. Rodzewicz, G. Czerwiński, and B.J. Kubica. Load spectrum – archiving, analysis and load sequences reproduction. *Proceedings of XIII Conference Mechanics in Aviation*, PTMTS, volume 1, pages 43–55, 2008. (in Polish).

[21] R. Fjortoft, Y. Delignon, W. Pieczynski, M. Sigelle, and F. Tupin. Unsupervised classification of radar images using hidden Markov chains and hidden Markov random fields. *IEEE Transactions on Geoscience and Remote Sensing*, 41(3):675–686, 2003. doi: 10.1109/TGRS.2003.809940.

[22] L.R. Rabiner. A tutorial on hidden Markov models and selected applications in speech recognition. *Proceedings of the IEEE*, 77(2):257–286, 1989. doi: 10.1109/5.18626.